Journal of Applied Fluid Mechanics, Vol. 18, No. 2, pp. 348-362, 2025.
Available online at www.jafmonline.net, ISSN 1735-3572, EISSN 1735-3645.
https://doi.org/10.47176/jafm.18.2.2862

Numerical Study on Static Airtightness of Subway Vehicles with Multiple Leak Holes

N. Li[1], H. Meng[2,3,4], T. Li[1†] and J. Zhang[1]

[1] *State Key Laboratory of Rail Transit Vehicle System, Southwest Jiaotong University, Chengdu 610031, China*
[2] *Beijing Infrastructure Investment Co., LTD, Beijing 100101, China*
[3] *Beijing Rail Transit Technology Equipment Group Co., LTD, Beijing, 100071, China*
[4] *Department of Mechanical Engineering, Tsinghua University, Beijing, 100084, China*

†Corresponding Author Email: litian2008@home.swjtu.edu.cn

ABSTRACT

In this study, a numerical simulation of the static leakage of a subway vehicle was conducted, based on the turbulence model of *k-ω* Shear Stress Transport (SST). The impact of the leak hole thickness and of the slenderness ratio, on the airtightness of the vehicle is analyzed with a single leak hole, as is the influence of the number, location, slenderness ratio, and area ratio of leak holes, on the airtightness of a train with multiple leak holes. The relative errors of the numerical simulation results are smallest when the leak hole slenderness ratio is 1:16. The relative errors in cases of a single leak hole, and of multiple leak holes are 4.93% and 3.68%, respectively. The pressure relief time first decreases, and then increases as the thickness of the leak hole increases, and is the smallest when the leak is 200 mm in thickness. Keeping the total area of leak holes unchanged, the location and number of leak holes have little impact on the pressure relief time. When door and window leak holes have different thicknesses, changing the area ratio of the door and window leak holes increases the pressure relief time, by a maximum of 1.23 seconds.

Article History

Received May 20, 2024
Revised July 5, 2024
Accepted August 29, 2024
Available online December 4, 2024

Keywords:

Subway vehicle
Static airtightness
Leakage hole
Leak characteristics
Numerical simulation

1. INTRODUCTION

In light of the trend of ever-increasing train operation speed, the requirements for train safety and comfort are also becoming increasingly onerous. (Raghunathan et al., 2002; Wei et al., 2024). When the train is traveling fast through a tunnel, a strong pressure wave will be generated (Saiprakash et al., 2019; Wu et al., 2022; Zhou et al., 2022), which will be transmitted to the interior of the train through gaps, such as doors and windows, causing pressure fluctuations in the train. As a train's service time increases, the train's air-tightness performance will decrease (Nam, 2004; Chen et al., 2021). Changes in external pressure will cause rapid changes in the internal pressure of the train, causing passengers to experience tinnitus, dizziness, and other uncomfortable symptoms (Gawthorpe, 1994; GlÖckle, 1994). To reduce the impact of pressure waves outside the train, on the air pressure inside the train, methods such as changing the track line spacing, changing the tunnel cross-sectional shape, and improving the airtightness of the train body are often used (Kobayashi et al., 1998; Hu et al., 2020; Lu et al., 2020). In order to ensure that the pressure fluctuations in the train meet requirements, a series of standards related to train airtightness have been formulated, both domestically and abroad, which stipulate the pressure change amplitude and pressure change rate in the train, when transient pressure changes occur outside the train. Su et al. (2004) presented the airtightness standards and airtightness test standards of high-speed trains in various countries, provided an overview of the current state of train airtightness research in various countries worldwide, and made a number of recommendations for our nation's airtightness research.

These days, several nations utilize dynamic and static airtightness indices, often known simply as airtightness indices, to assess how airtight a train is. Typically, the dynamic airtightness index is two or three times higher than the static airtightness index. In terms of theoretical and experimental research on train airtightness, Li and Mei (2009) measured the change curve of the pressure inside and outside the vehicle, through experimentation, and then calculated the airtightness constant of the train through theoretical formulae. They also used the established analysis program, to verify the test data of the airtightness of different vehicles. Liu et al. (2017, 2019) experimentally tested the changes in pressure within the

NOMENCLATURE

A	cross-sectional area of the leak hole	v	central velocity of the leak hole section
A_i	cross-sectional area of each leak hole	v_i	center velocity of each leak hole
p_e	air pressure outside the car	y^+	non-dimensional wall distance for a wall-bounded flow
p_i	initial air pressure inside the car	y^+	non-dimensional wall distance for a wall-bounded flow
Q_m	gas mass flow rate	α	flow coefficient of the leakage hole
Q_{mi}	gas mass flow rate of each leak hole	γ	specific heat capacity ratio of air
R	gas constant of air	Δp_1	initial pressure difference between the vehicle's interior and exterior
S_r	slenderness ratio	Δp_2	pressure difference at the end of the pressure relief
T_e	temperature of the outside air	λ	A coefficient that takes the value of 1in the paper
t_s	pressure relief time	ρ_e	density of the outside air
V	volume capacity of the leakage body	τ_s	static airtightness index

train when it passed through tunnels of different lengths, and obtained the variation pattern of dynamic airtightness index, with tunnel length. Xu et al. (2014) monitored the internal pressure changes of trains running on open lines under different working conditions. Based on the airtightness index, they identified the law of dynamic airtightness index change with running time. Full-scale testing and wind tunnel testing can better test the aerodynamic performance parameters of the train (Li et al., 2023), but the test cost is high, and the test conditions are limited. Therefore, Numerical simulations are widely used to study train aerodynamics (Chang et al., 2021; Liang et al., 2022). Li et al. (2020) derived the train static airtightness leakage equation, considering the leak hole flow coefficient. Through numerical simulation analysis, the impact of the leak hole slenderness ratio and the initial air pressure within the train, on the static airtightness was compared. The theoretical formula was compared with the results of numerical simulation, and it was proven that the theoretical formula can be used to calculate the static leakage time of the train. Nam (2016) used the airtightness index, to numerically calculate the pressure changes inside the train. The difference between the calculated and experimental outcomes was small, which shows that numerical simulation is accurate in calculating train airtightness. Li et al. (2022) studied the pressure comfort inside a subway vehicle when it passes through a subway station, conducted a comparative analysis of different airtightness indicators of the train, and gave suggestions for mitigating the pressure changes inside the vehicle, when it passes through a station. Liu et al. (2020) employed numerical simulation to investigate the impact of various factors, including pressure frequency and amplitude, on the outer surface of the train, the scale of the model, and equivalent leakage area, on the dynamic airtightness of the train. They found the relationship between these parameters, and the dynamic airtightness. Through fluid-solid coupling simulation, Chen et al. (2022) established a model of the influence of three factors, being train deformation, clearance, and air duct opening, on the airtightness of the car body under tunnel pressure wave excitation, and validated their model's applicability. Niu et al. (2023) established a proxy model of key parameters of trains and tunnels, and combined it with numerical simulation to verify the accuracy of the model, which can be used to optimize and predict the airtightness parameters of trains and tunnels, for engineering applications. In addition to studying the airtightness of trains, through experiments and numerical simulations, He et al. (2022, 2023) used an iterative learning control (ILC) algorithm to control the air pressure inside the train when passing through a tunnel. This method is more suitable for achieving ride comfort.

At present, relevant research mainly focuses on evaluating the static airtightness index of trains, from a theoretical and experimental perspective, while simulation research involving the static airtightness of trains is relatively limited. The gap in the train body is a key factor affecting airtightness. Since the leakage gaps of different types of trains vary greatly, the theoretical formulae may have large errors in calculation. Therefore, this paper takes the static airtightness of subway trains as the research object, and uses numerical simulation methods to study the impact of parameters, such as slenderness ratio, thickness, quantity, and the location of body leak holes, on the static airtightness of the train. This study enables more detailed understanding of the impact of different leak hole parameters on the static airtightness of trains, and provides theoretical and practical suggestions for improving the airtightness performance of trains.

2. NUMERICAL INFORMATION

2.1 Calculation Method of Static Airtightness

When testing the static airtightness of trains, the inflation leakage method is generally used. The method is to introduce gas to the carriage to reach an initial air pressure, then release the pressure through the leak hole, and record the time it takes for the pressure in the carriage to decrease from the initial pressure difference Δp_1, to Δp_2, to obtain the static airtightness index of the train. The static airtightness index is calculated as follows:

$$\tau_s = \frac{t_s}{\ln(\frac{\Delta p_1}{\Delta p_2})} \tag{1}$$

where τ_s is the static airtightness index, Δp_1 is the initial pressure difference between the vehicle's interior and exterior, Δp_2 is the pressure difference between the vehicle's interior and the exterior, at the end of pressure relief, t_s is the time it takes for the pressure difference between the vehicle's interior and exterior to drop from Δp_1 to Δp_2.

Since this formula requires the pressure relief time to be obtained through experiments or simulation, it is impossible to directly estimate the static airtightness index of trains. Therefore, the theoretical calculation Eq. (2), based on the box leakage model and taking into account the leak hole flow coefficient, can be used to directly calculate the pressure relief time of static leakage (Li et al., 2020).

$$t_s = \frac{\sqrt{2}V(\sqrt{\Delta p_1} - \sqrt{\Delta p_2})}{\lambda \alpha \gamma R A T_e \sqrt{\rho_e}} \tag{2}$$

where V is the volume capacity of the leakage body, α is the flow coefficient of the leakage hole, the magnitude of which is related to the geometric parameters of the leak hole, γ is the specific heat capacity ratio of air, 1.4, R is the gas constant of air, R=287.06 J/(kg·K), A is the cross-sectional area of the leak hole, T_e is the temperature of the outside air, and ρ_e is the density of the outside air.

The coefficient λ is related to the specific heat ratio of air, and to the pressure inside and outside the car. Since the gas in the leak hole is affected by wall friction and by viscosity when flowing, the velocity near the edge of the hole is low, while the velocity at the center of the hole is high, so the gas flow rate in the cross-section of the leak hole is large at the center, and small near the edge. Therefore the theoretical calculation takes into account the flow coefficient, required to analyze the leak hole. The calculation formulae of coefficient λ and flow coefficient α are as follows

$$\lambda = (1 + \frac{\gamma - 1}{\gamma} \frac{p_i - p_e}{p_e}) \Bigg/ \sqrt{1 + \frac{1}{\gamma} \frac{p_i - p_e}{p_e}} \tag{3}$$

$$\alpha = \frac{Q_m}{vA} \tag{4}$$

where p_i and p_e are the vehicle's internal initial pressure and external pressure, respectively, Q_m is the gas mass flow rate through the leak hole section, and v is the central velocity of the leak hole section.

Regarding the research on the static airtightness of trains, since the value of atmospheric pressure outside the car is large, the ratio of the pressure difference between the vehicle's interior and exterior, to the atmospheric pressure outside the car is small, so it can be approximated that λ = 1.

2.2 Numerical Simulation Model

A single-car model of a subway vehicle is used as the numerical simulation model. The single-car model is relatively simple, which significantly reduces the computational complexity and resource requirements, but can still provide an in-depth understanding of the impact of leak holes on leakage characteristics. Figure 1(a) shows the calculation domain. The four sides and the top surface of the calculation domain are the pressure outlet boundaries, the outlet pressure is 0, and the ground and the carriage are both stationary walls. As shown in Fig. 1(b), the length, width, and height of the carriage are 22.0, 2.8, and 2.3 m, respectively, and the volume of the interior domain is 131.4 m^3. Fig. 1(c) shows the 2D view of the computational domain partition of the x = 0 cross-section. The computational domain was divided into the interior air and the exterior atmosphere calculation domains. The interior of the carriage is connected to the outside atmosphere through the leak hole, and data passing between the two computational domains is transferred using the interface. The cross-sectional area of the leak hole on the cabin is 2638 mm^2. The initial air pressure in the cabin is 2600 Pa, and the pressure relief time for the air pressure in the car to drop from the initial pressure to 1000 Pa, is used as the static airtightness evaluation standard.

The static leaking of the carriage was numerically simulated using the turbulence model of the k-ω Shear Stress Transport (SST) turbulence model, to more accurately determine the turbulent structure around the leak hole wall (Li et al., 2019a, b). The Second Order Upwind format, in discrete format, is used for the calculation, to ensure accuracy. A time step of 0.002 s was used for the transient calculation, the number of time steps was 10000, and the total calculation time was 20 s.

3. NUMERICAL VALIDATION

3.1 Mesh Independence

Figure 2 illustrates the meshing results. Figure 2(a) shows the surface meshes of the train and the leak hole, and Fig. 2(b) shows the 2D meshes of the x = 0 cross-section in the computational domain. A mixed mesh of tetrahedrons and hexahedrons was used for meshing. Three refinement zones were divided near the leak hole and the carriage, and the boundary layer meshes were divided near the wall of the leak hole. The height of the first boundary layer was 0.1 mm, and there were 8 boundary layers in total, satisfying the requirement of y^+ ＜1. A model with a leak hole slenderness ratio of 1:8 was meshed. Three sets of finite element models with different mesh numbers were divided, with basic dimensions of 2000 mm, 1800 mm, and 1600 mm, and named Mesh 1~3. Numerical simulations were performed using these finite element models, and the pressure relief times, during which the pressure in the vehicle reduced from 2600 Pa to 1000 Pa, were compared between models. Table 1 lists the parameters and pressure relief times of the three sets of meshes. Figure 3 shows the comparison of the in-vehicle pressure time history curves and the leak hole cross-section mass flow rate time history curves, of the three sets of meshes.

The table shows that as the number of meshes increases, the pressure relief time decreases, to a certain extent. The pressure relief time of Mesh 2 is reduced by 0.33% compared to Mesh 1, and the pressure relief time of Mesh 3 is reduced by 0.12% compared to Mesh 2. It can

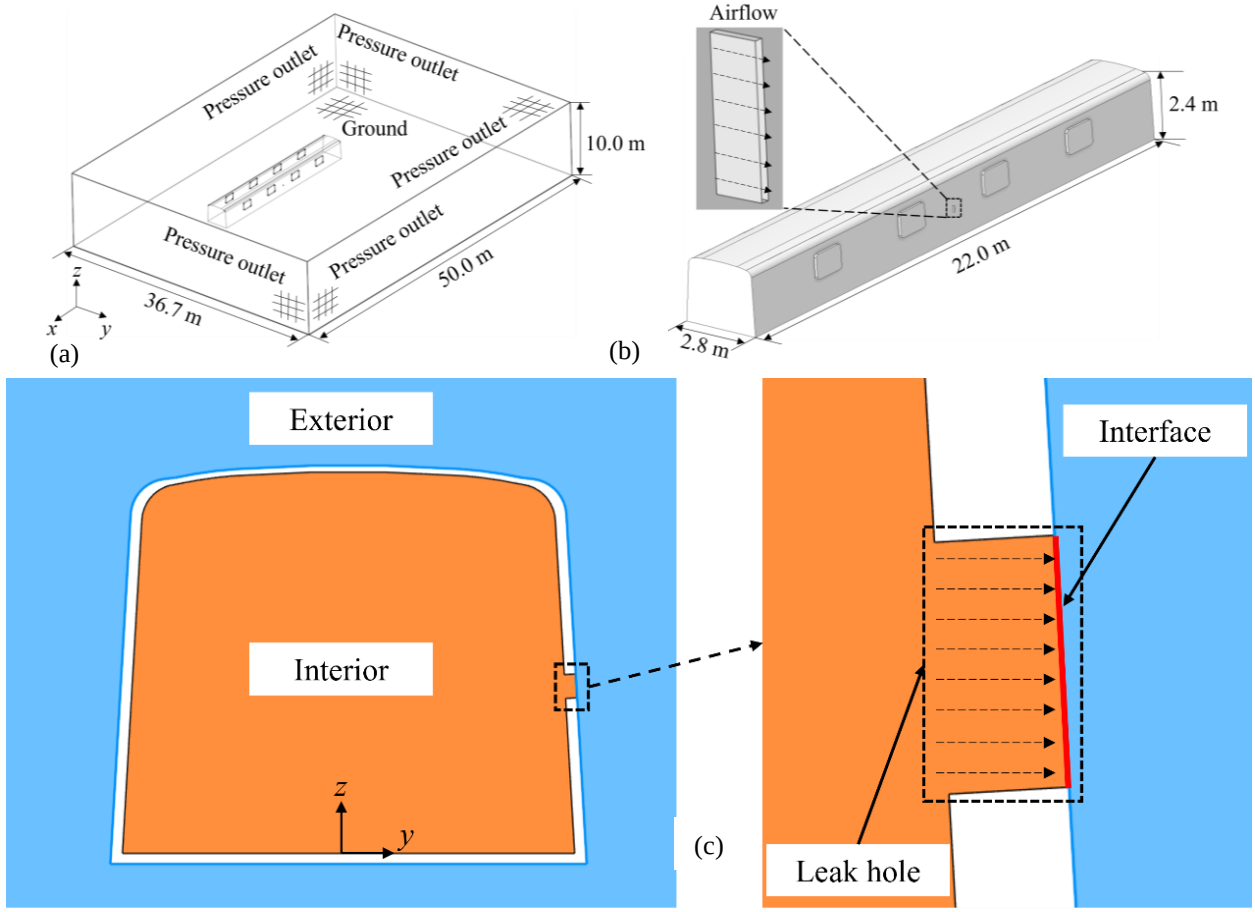

Fig. 1 Numerical simulation model: (a) Computational domain and boundary conditions; (b) Carriage and leak hole model; (c) 2D view of the computational domain partition of the x = 0 section

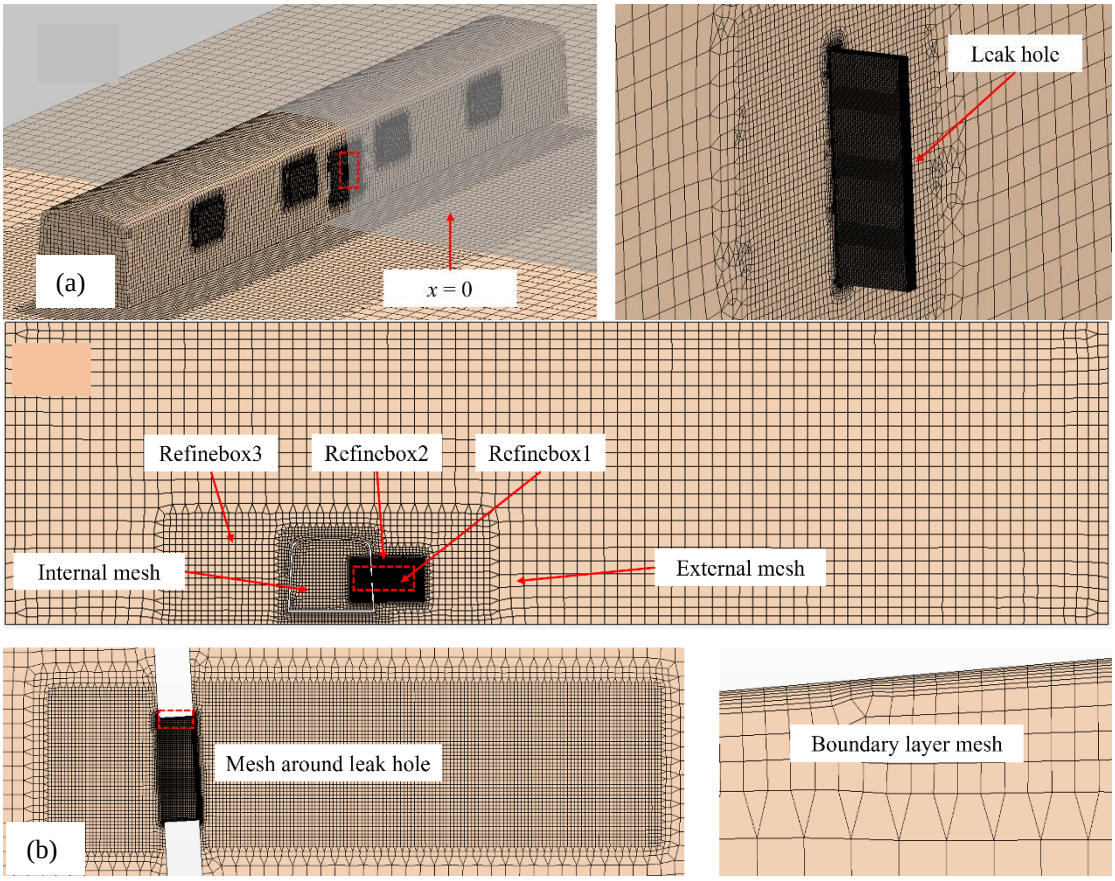

Fig. 2 Mesh of computational domain: (a) 3D view meshes; (b) 2D view meshes for x = 0 section

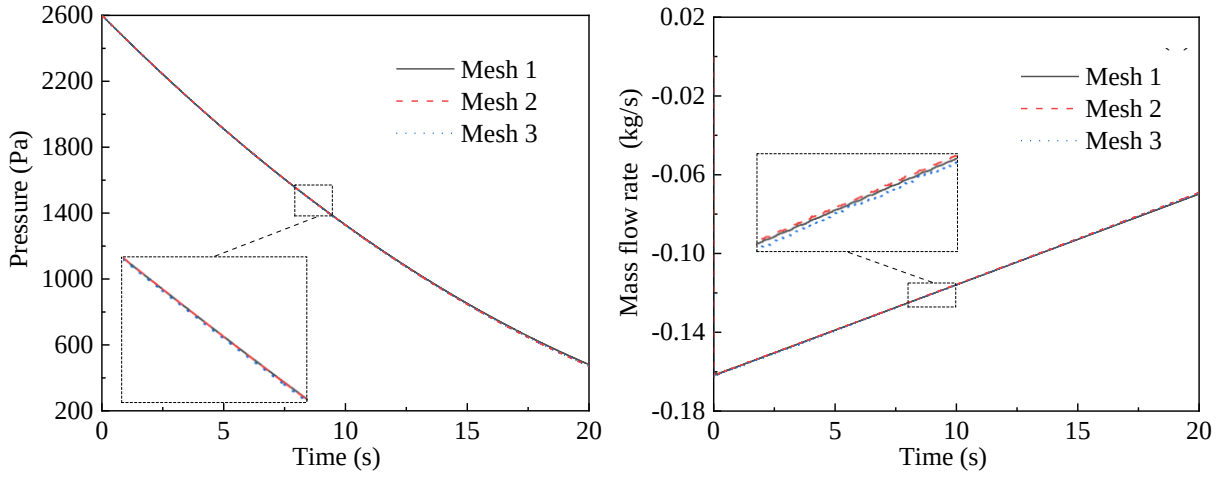

(a) (b)

Fig. 3 Comparison of leakage characteristics of different meshes: (a) Pressure time history curve inside the carriage; (b) Mass flow rate curve of the leak hole

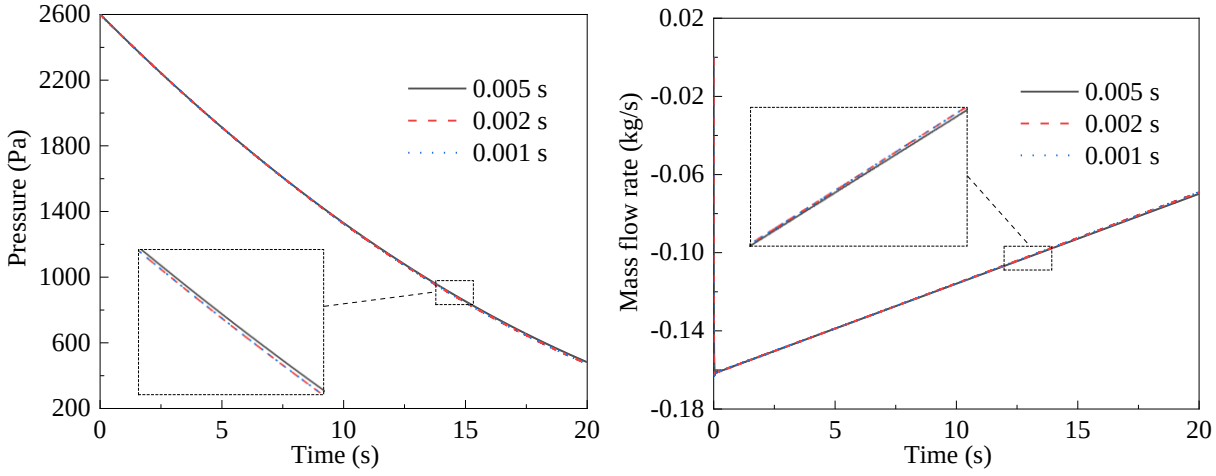

(b) (b)

Fig. 4 Comparison of leakage characteristics of different time steps: (a) Pressure time history curve inside the carriage; (b) Mass flow rate curve of the leak hole

Table 1 Comparison table of mesh independence validation

	Mesh 1	Mesh 2	Mesh 3
Basic size (mm)	2000	1800	1600
Number of meshes (10^4)	206	256	334
Pressure relief time (s)	13.32	13.28	13.26
Computation time (h)	50.0	61.1	83.3

be seen that when the number of meshes exceeds 2.56 million, pressure relief time varies very little with the number of meshes. As shown in Fig. 3, the differences between the pressure time history curves of the three sets of meshes, and the mass flow rate curves of the leak hole cross-section are very small, and the curves are essentially consistent. The computation times for these three meshes are about 50.0 h for Mesh 1, 61.1 h for Mesh 2, and 83.3 h for Mesh 3, respectively. As a result, continuing to refine the mesh will hardly affect the static leakage characteristics of the train, but will increase the computation time. Considering the calculation speed and accuracy, subsequent simulations will use the basic mesh size of Mesh 2, to mesh and conduct calculations.

3.2 Time Step Independence

In order to validate that differences in time step do not significantly affect the results, different time steps were selected for numerical simulation, which were 0.005, 0.002, and 0.001 s. Figure 4 shows the comparison of the in-vehicle pressure time history curves and the leak hole cross-section mass flow rate time history curves, using the different time steps. It can be seen that the differences between the pressure and mass flow rate profiles at the three different time steps are very small. The pressure relief times for time steps of 0.005, 0.002, and 0.001 s were about 13.34, 13.32, and 13.32 s, respectively, and the pressure relief times calculated by time steps of 0.002 s and 0.001 s were almost the same. Therefore, the time step of 0.002 s was chosen for subsequent calculations.

3.3 Validation of Test

The comparison of the experimental and the numerical simulation results was used to validate the accuracy and reliability of the numerical simulation. The

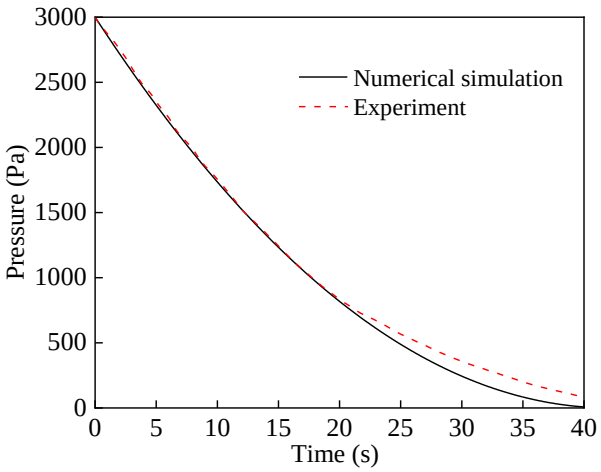

Fig. 5 Comparison of test and numerical simulation results

test used a cabin model with an internal volume of 108 m^3. It was filled with high-pressure gas, to make the internal pressure of the cabin 3000 Pa higher than atmospheric pressure. Then, static pressure relief was performed, and the curve of the pressure inside the cabin was recorded. The test data results come from the literature (Li et al., 2009).

Figure 5 compares the vehicle interior pressure time history curves from the experiment, and from the numerical simulation. In the first 20 seconds, the pressure curves of the numerical simulation and the experiment are mostly consistent, but as the pressure in the car decreases, the difference in the pressure curves gradually becomes larger. This may be because the external atmospheric pressure set in the numerical simulation is 0, which is an ideal value. However, the atmospheric pressure of the test environment is affected by the geographical location. The atmospheric pressure in the test may be slightly higher than the atmospheric pressure set by the numerical simulation. As the pressure difference between the vehicle's interior and exterior decreases, the error between the simulation and test results increases. Therefore, when the pressure difference between the vehicle's interior and exterior is greater than a certain value, the results of numerical simulation are more accurate. In view of the influence of the pressure difference between the inside and outside of the train on the results, and the static airtightness evaluation index of subway vehicles, this article uses pressure relief time as the evaluation criterion for the static airtightness of the train. Here, the pressure relief time is the time during which the pressure difference between the inside and outside of the train drops from 2600 Pa to 1000 Pa.

4. Results And Discussion

4.1 Analysis of Influencing Factors on Train Airtightness Under Single Leak Hole Condition

4.1.1 Slenderness Ratio of Leak Hole

The cross-sectional parameters will affect the flow coefficient of the leak holes, which in turn affects the static pressure relief time. Therefore, five rectangular leak hole models, with different slenderness ratios were established,

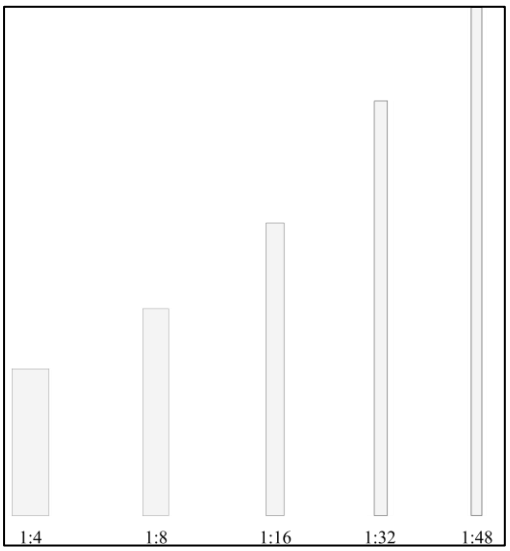

Fig. 6 Leak holes with different slenderness ratios

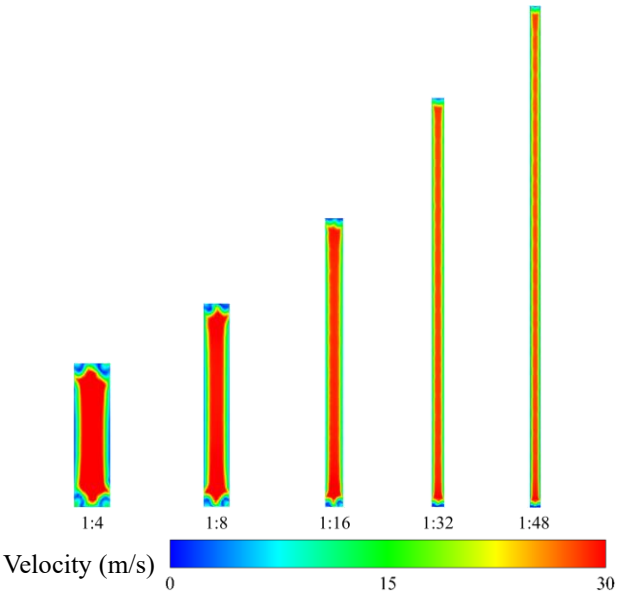

Fig. 7 Velocity distribution of leak hole cross-section

and their slenderness ratios were 1:4, 1:8, 1:16, 1:32, and 1:48, respectively. The cross-sectional area of the leak hole was 2638 mm^2. Numerical simulations were carried out on the above leak hole model. Due to the different slenderness ratios of the leak holes, the flow coefficients of various leak holes are different. The cross-sectional mass flow rate and cross-sectional center velocity of the leak holes were obtained through numerical simulation, and the flow coefficient of each leak hole could be calculated using Eq. (4). Then, the pressure relief time of leak holes with different slenderness ratios could be calculated according to Eq. (2), and compared with the pressure relief time obtained by simulation. In Eq. (2), Δp_1 and Δp_2 are 2600 Pa and 1000 Pa, respectively, and the temperature and density of the air outside the car are 288.15 K and 1.225 kg/m^3, respectively.

Table 2 shows the comparison of the pressure relief time of leak holes with different slenderness ratios. As the slenderness ratio of the leak hole decreases, the flow coefficient of the leak hole gradually increases, so the theoretical pressure relief time decreases. Figure 7

Table 2 Comparison of pressure relief time of leak holes with different slenderness ratios

Slenderness ratio	1:4	1:8	1:16	1:32	1:48
Flow coefficient	0.70	0.74	0.76	0.77	0.77
Theoretical pressure relief time (s)	15.21	14.39	14.01	13.83	13.83
Numerical simulation pressure relief time (s)	13.48	13.28	13.32	12.99	13.13
Relative error	11.37%	7.71%	4.93%	6.07%	5.06%

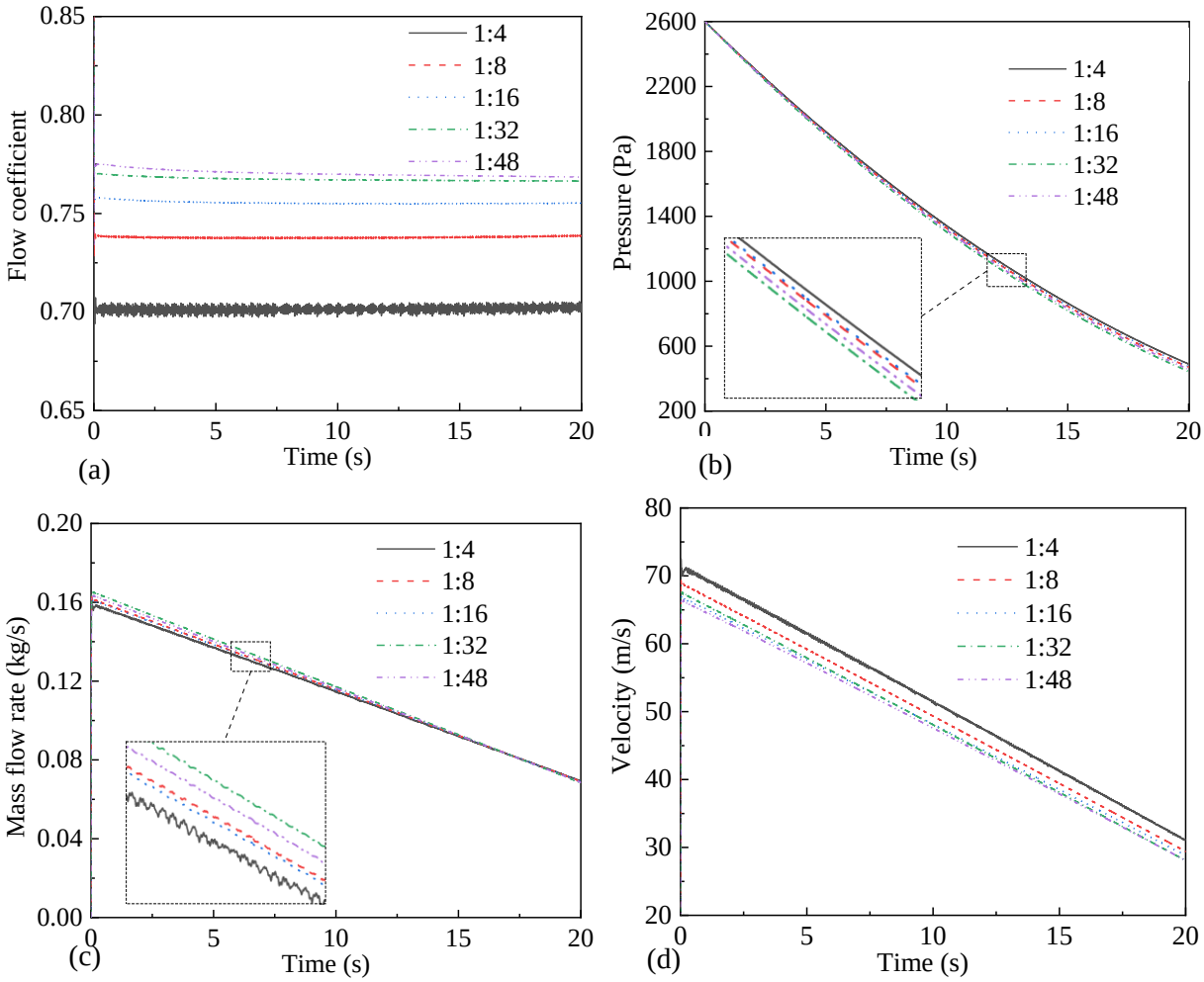

Fig. 8 Comparison of leakage characteristics of leak holes with different slenderness ratios: (a) Flow coefficient; (b) Pressure inside the carriage; (c) Mass flow rate; (d) Central velocity of leak hole

illustrates the velocity distribution of the cross-section of the leak hole at t = 20 s. As the slenderness ratio of the leak hole decreases, the central velocity of the leak hole decreases, resulting in a more uniform velocity distribution across the cross-section, so the flow coefficient of the leak hole increases. As the slenderness ratio decreases from 1:4 to 1:16, the relative error between the pressure relief times obtained from numerical simulation and the theoretical time, gradually decreases. The relative error of the leak hole with a slenderness ratio of 1:16 is only 4.93%.

By analyzing the numerical relationship between the flow coefficients and slenderness ratio in Table 2, the fitting formula between the flow coefficients and slenderness ratio, as shown in Eq. (5), was obtained. The R^2 of this fitting equation is 0.9999, which indicates the accuracy of the fitting equation.

$$\alpha = -0.3199 S_r + 0.7799 \tag{5}$$

where S_r is the slenderness ratio.

It is evident from Fig. 8, that the flow coefficient is less affected by changes in pressure inside the car. As the leak time increases, the flow coefficient changes little. The pressure curves in the car with leak hole slenderness ratios of 1:8 and 1:16 are relatively consistent, indicating that the simulation results obtained by using the leak hole with the slenderness ratio of 1:16 are more reliable. The central velocity and mass flow rate of the leak hole cross-section (the sign of the mass flow rate indicates the flow direction of the gas), both decrease with the increase of leak time, and have a linear relationship with time. The central velocity of the leak holes, (taken at the same time), decreases as the slenderness ratio of the leak holes decreases, corresponding to the velocity distribution pattern in Fig. 7.

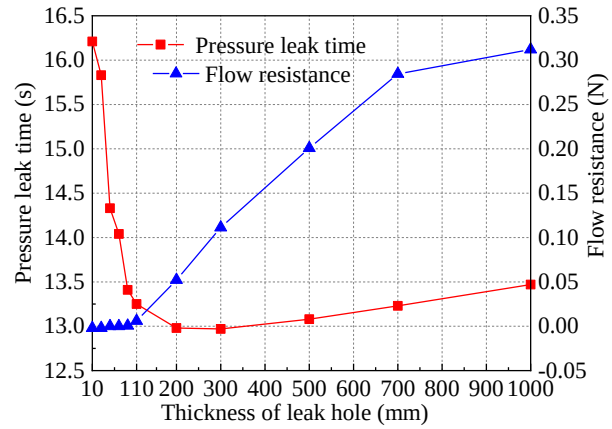

(a)

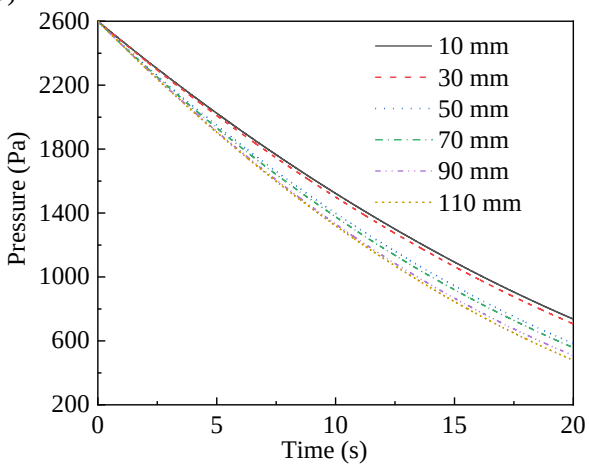

(b)

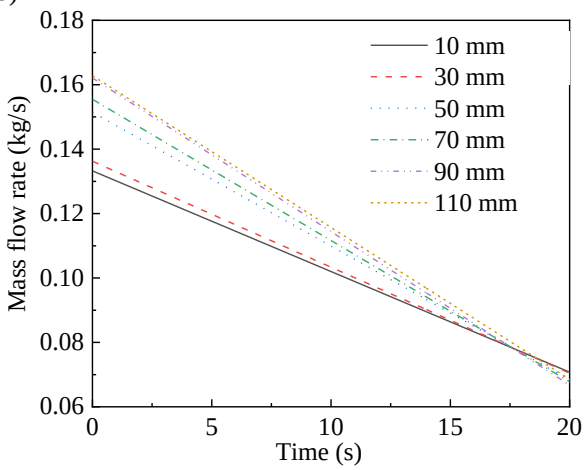

(c)

Fig. 9 Comparison of leakage characteristics of leak holes with different thicknesses: (a) Pressure relief time and flow resistance; (b) Pressure inside the carriage; (c) Mass flow rate

4.1.2 Thickness of Leak Hole

The thickness of the train body is inconsistent, due to different structures, so the thickness of the leak holes in the body is also inconsistent. To investigate the impact of leak hole thickness on the static leakage characteristics of the train, the short leak hole models (where the thickness of leak holes are 10 mm, 30 mm, 50 mm, 70 mm, 90 mm, and 110 mm, respectively), and the long leak hole models (where the thickness of leak holes are 200 mm, 300 mm, 500 mm, 700 mm, and 1000 mm, respectively), with the slenderness ratio of 1:16, were established for numerical simulation. The thickness of the leak hole in the real car body will not be very large. The reason why the leak hole value in this research is larger, is to study the change law of static leakage characteristics, as the thickness of the leak hole increases.

Figure 9(a) shows how the pressure relief time, and the flow channel viscous resistance, change with the thickness of the leak hole. It can be seen that when the thickness of the leak holes is less than 200 mm, the pressure relief time reduces with increases in the thickness of the leak holes. When the thickness of the leak holes is greater than 200 mm, the pressure relief time increases with increases in the thickness of the leak holes. When the thickness of the leak holes is less than 110 mm, the wall resistance is small. When the thickness of the leak holes is greater than 110 mm, the wall resistance of the leak hole increases almost linearly with the thickness of the leak holes. Figure 9(b) and (c) show the pressure change curves inside the cabin, and the mass flow rate curves of leak holes of sizes less than 110 mm. As the thickness of the leak holes increases, the leak hole mass flow rate gradually increases, and the slope of the mass flow rate curves increases with increases in the thickness of the leak holes, so that the gas leaks faster. The mass flow rates of the leak holes with varying thicknesses converge as the leakage time approaches 17.5 seconds.

Figure 10 shows the longitudinal velocity distribution of some leak holes at t = 10 s. It is clear that the airflow velocity in the leak hole channel becomes larger, and the pressure relief time becomes shorter, as the thickness of the leak holes increases up to 200 mm. When the thickness of the leak holes is greater than 200 mm, as the thickness continues to increase, the airflow speed no longer becomes larger, but the wall viscosity resistance increases, so the airflow velocity decreases, and the pressure relief time increases.

From the above analysis, it can be seen that if the thickness of the leak holes is too small, the gas will not have time to accelerate in the flow channel. Therefore, the increase in the thickness of the leak holes can increase the airflow velocity, and shorten the pressure relief time. When the thickness of the leak holes is greater than 200

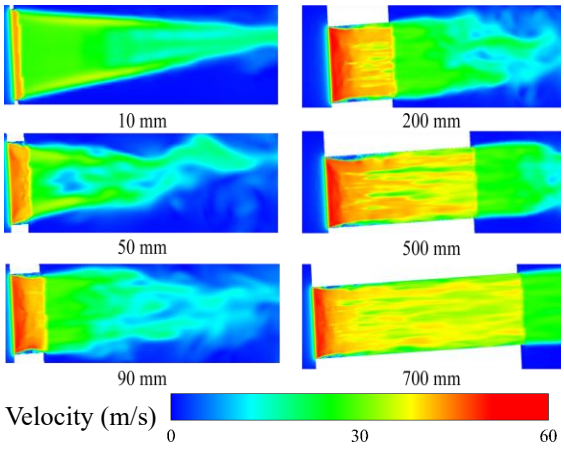

Fig. 10 Velocity distribution of the longitudinal section of the leak holes

mm, the viscous resistance of the flow channel represents the primary factor influencing the leak time. The increase in viscous resistance will cause the overall airflow velocity in the leak holes to decrease, and the pressure relief time to become longer.

4.2 Analysis of Influencing Factors on Train Airtightness Under Multiple Leak Hole Condition

4.2.1 Number and Location of Leak Holes

The number and location of the leak holes distributed on a car body will be different. The different distribution of leak holes on the carriage was simulated, a porous leakage car body model was established, and the impact of the number and spatial distribution of leak holes on the model's leakage characteristics was studied. The number and location distribution of different leak holes are shown in Fig. 11. The leak holes are all symmetrically distributed. In Fig. 11(a), N1, N2, N4, and N8 depict the cases where the number of leak holes in the carriage is 1, 2, 4, and 8, respectively. Except for case N8, which has 4 door leak holes and 4 window leak holes, other cases only have door leakage holes. The leak hole areas of the doors and windows are allocated according to the perimeter ratio of the doors and the windows. The total area of leak holes in all different cases is 2638 mm^2. The area sizes of the leak holes for each case are shown in Table 3. The distribution positions of different leak holes are shown in Fig. 11(b). N8_V1 and N8_V2 represent the distribution of leak holes at two different positions in case N8, respectively. The door leak holes are named D1~D4, and the window leak holes are named W1~W4.

Table 3 The area of the leak holes in different cases

	N1	N2	N4	N8	
Type of leak hole	door	doors	doors	doors	windows
Area of single leak hole (mm^2)	2638	1319	659.5	382.7	276.8
Number of leak holes	1	2	4	4	4
Total leakage hole area (mm^2)	2638	2638	2638	2638	

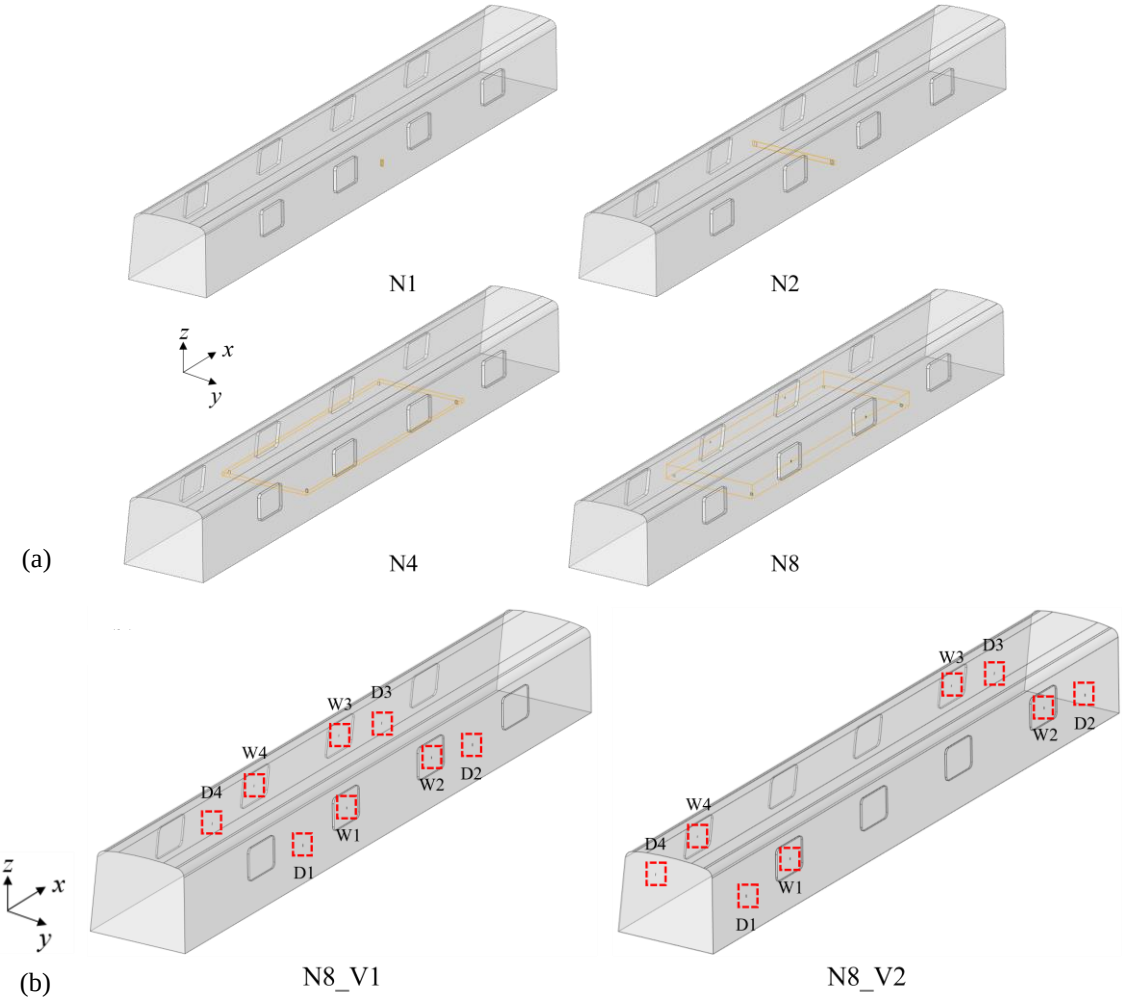

Fig. 11 Distribution of leak holes in different numbers and locations: (a) Different numbers of leak holes; (b) Different locations of leak holes

Figure 12 shows the comparison of leakage characteristics with varying numbers of leak holes. It is evident from Fig. 12(a) that the different number of leak holes has little impact on pressure leakage, and the pressure time history curves are nearly the same. A slight discrepancy is observed in the mass flow rate curves, which may be because of the difference in the airflow velocity in the leak holes, itself due to the different area sizes of a single leak hole under different cases. The pressure relief times of cases N1~N8 are 14.04, 13.90, 13.80, and 13.94 seconds, respectively. The maximum difference in pressure relief times is only 0.24 s. The effect of the number of leak holes on the pressure relief time is less than 2%.

Figure 12(c) and Fig. 12(d) compare the mass flow rate and flow coefficient change curves of each door and window leak hole, under case N8. It is clear that since the areas of leak holes of the same type are identical, there is very little difference in mass flow curves for the same type of leak hole. It can be seen that the values of the flow coefficients have specific differences between the four door leak holes, these vary between 0.84 and 0.87. The flow coefficients of different window leak holes are almost the same, about 0.54. Figure 13 shows the velocity distribution of the cross-section, and the longitudinal section of the leak holes, respectively. It can be seen that the section velocity distributions of the same leak holes are identical, and the velocity of the cross-section is distributed with a large center and small surroundings. Therefore, the difference in the flow coefficients of the same leak holes is small, but because the area of the window leak holes being smaller, their flow coefficients are smaller.

Figure 14 shows the comparison of leakage characteristics after changing the distribution position of door and window leak holes. The time history curves of the interior pressure of the two different leak hole positions overlap. Changing the position of the leak holes will not affect the leakage time. However, a minor discrepancy is present in the mass flow rate curves of the same leak holes, after changing the positions. The mass flow rate of the door leak holes in case V1 is slightly smaller than that in case V2, and the mass flow rate of the window leak holes in case V1 is slightly larger than that in case V2. After changing the positions of the leak holes, the changes in the mass flow rate of the door and window are reversed, so it has less impact on the pressure relief time.

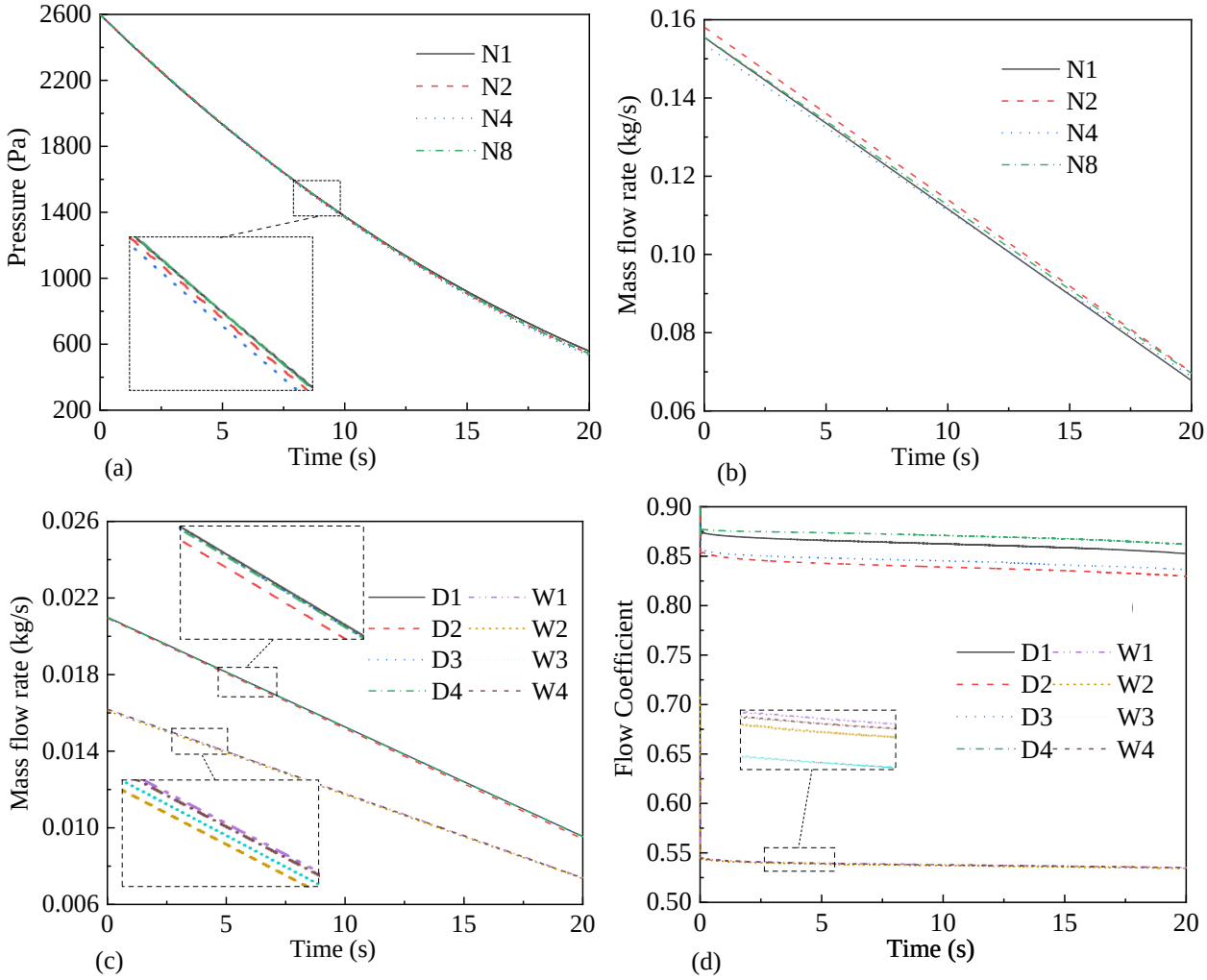

Fig. 12 Comparison of leakage characteristics with different numbers of leak holes: (a) Pressure inside the carriage; (b) Mass flow rate; (c) Mass flow rate of doors and windows leak holes of case N8; (d) Flow coefficient of doors and windows leak holes of case N8

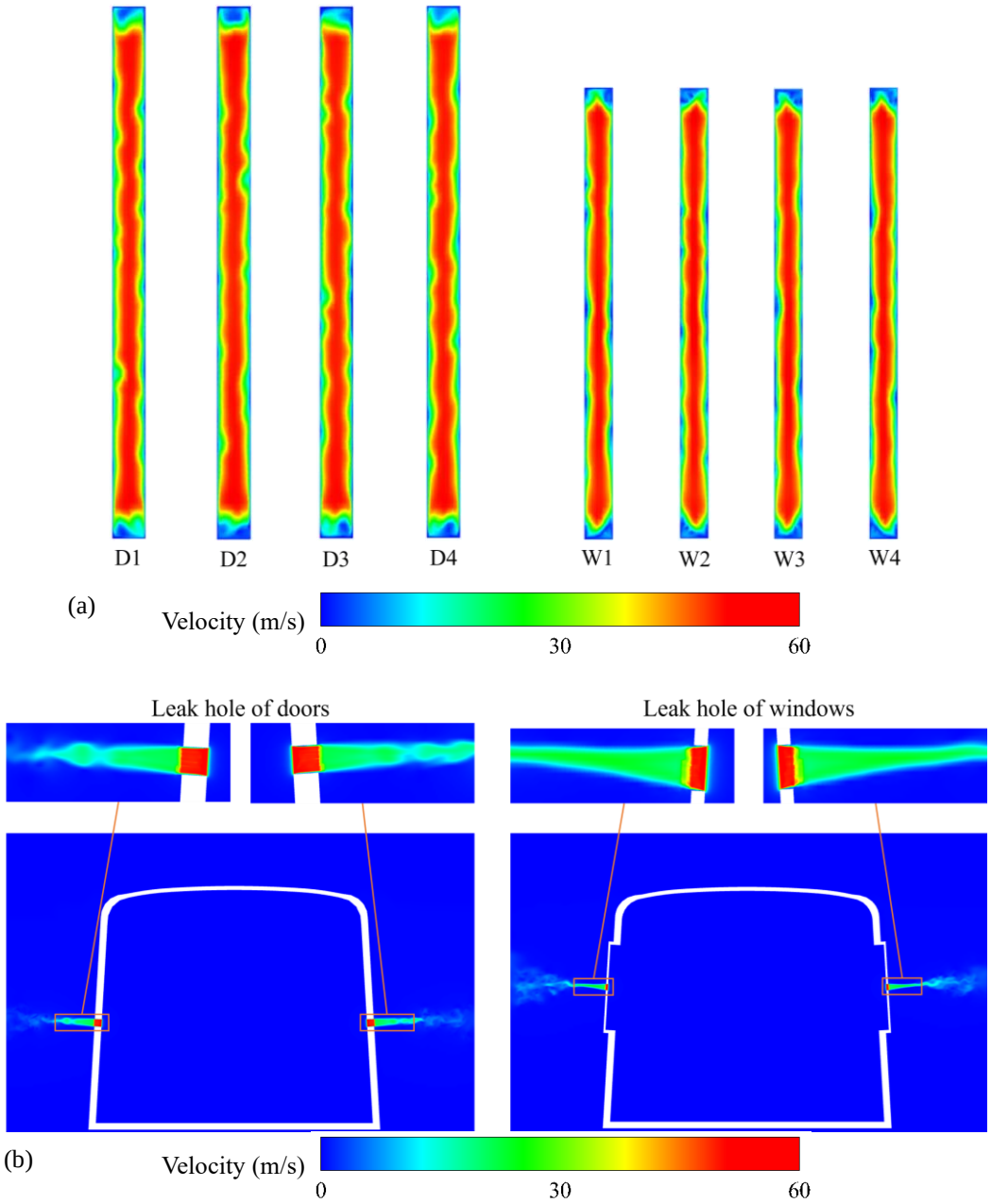

Fig. 13 Velocity distribution of doors and windows leak holes of case N8: (a) Velocity distribution of cross-section of leak holes; (c) Velocity distribution of longitudinal section of leak holes

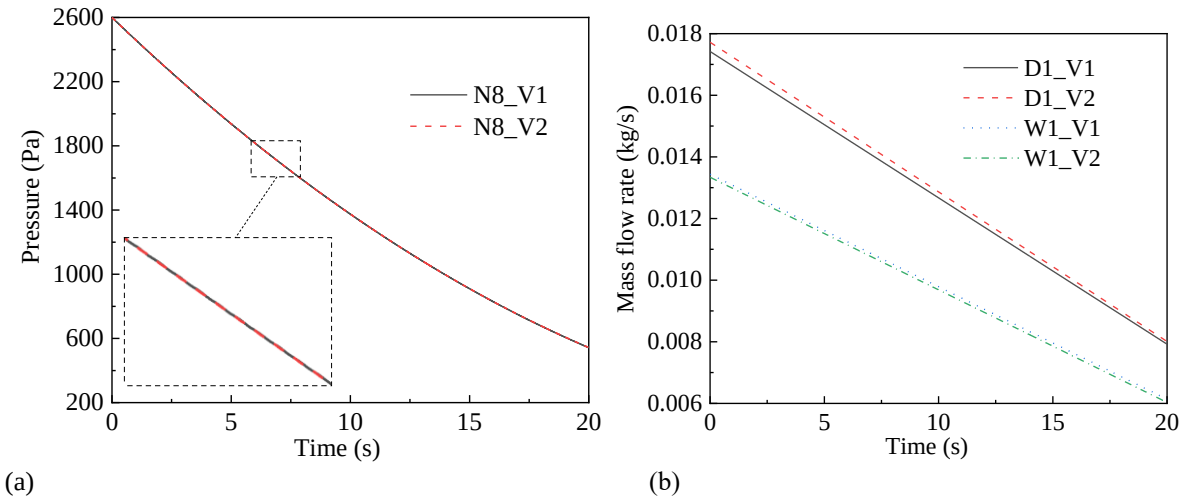

Fig. 14 Comparison of leakage characteristics with different locations of leak holes: (a) Pressure inside the carriage; (b) Mass flow rate of doors and windows leak holes

Table 4 Comparison of pressure relief time of leak holes with different slenderness ratios

Slenderness ratio	1:4	1:8	1:16
Flow coefficient	0.74	0.75	0.80
Theoretical pressure relief time (s)	14.39	14.20	13.31
Numerical simulation pressure relief time (s)	13.67	13.64	13.80
Relative error	5.00%	3.94%	3.68%

Table 5 Leak hole area for different area ratios

Area ratio	Area of door leak holes (mm^2)	Area of window leak holes (mm^2)
3:1	494.66	164.89
2:1	439.69	219.85
1.38:1 (Original)	382.81	276.73
1:1	329.77	329.77
1:2	219.85	439.69
1:3	164.89	494.66

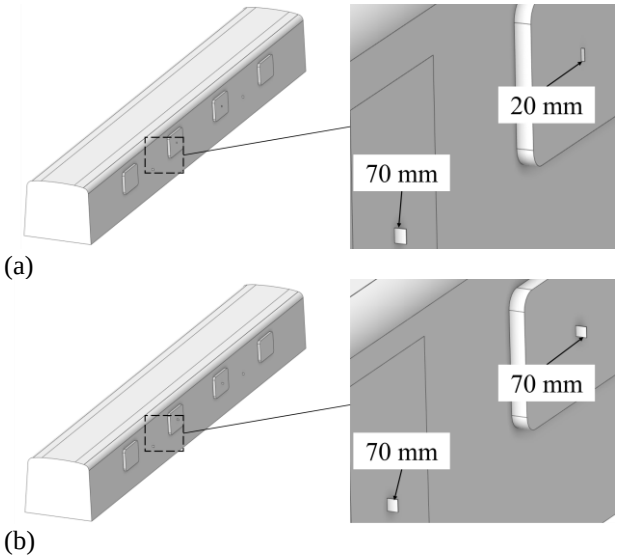

Fig. 15 Thickness of leak holes in doors and windows: (a) Different door and window leak hole thickness (b) Same door and window leak hole thickness

4.2.2 Slenderness Ratio of Leak Hole

Numerical simulations were conducted on case N8 with leak hole slenderness ratios of 1:4, 1:8, and 1:16, respectively. The flow coefficients of the leak holes were calculated using the same method as for single-hole leakage, and the pressure relief time was compared between theoretical calculation, and numerical simulation. The flow coefficient calculation formula for porous leakage is as follows:

$$\alpha = \frac{\sum Q_{\mathrm{mi}}}{\sum v_{\mathrm{i}} A_{\mathrm{i}}} \tag{6}$$

where Q_{mi} is the gas mass flow rate of each leak hole cross-section, v_{i} is the center velocity of each leak hole cross-section, A_{i} is the cross-sectional area of each leak hole.

It can be seen from Table 4 that the flow coefficient for the same slenderness ratio with multiple leak holes, is larger than that with a single leak hole. When there is only one leak hole in the car, the area of the leak hole is larger, and the airflow in the center of the hole is less affected by wall viscosity, so the center velocity is larger. When a single leak hole is split into multiple leak holes distributed on the carriage surface, the area of each leak hole decreases, so the airflow in the center of the hole is more affected by wall viscosity, and the center velocity is smaller. Therefore, under the same slenderness ratio, the hole center velocity in the case of leakage from multiple leak holes is smaller than that of leakage from a single leak hole, the theoretical flow rate is smaller, and the flow coefficient is larger.

As the slenderness ratio of the leak holes decreases, the flow coefficients of the leak holes gradually increase, and the difference in pressure relief time obtained by numerical simulation is small. In the case of porous leakage, the slenderness ratio of the leak hole has a less than 2% impact on the pressure relief time. The relative error in pressure relief time, between the theoretical calculation and the simulation, decreases as the leak hole slenderness ratios decrease. When the leak hole slenderness ratio is 1:16, the relative error is only 3.68%, smaller than in the case of single hole leakage.

4.2.3 Area Ratio of Doors and Windows Leak Holes

For different vehicles, the specifications of the doors and windows are different, so the area ratio of the doors and windows leak holes is also distinct. The total area of leak holes was kept unchanged, while the area ratio of leak holes in doors and windows was varied, to study the impact on vehicle leakage characteristics. The area sizes of leak holes with different area ratios are shown in Table 5. Since the thickness of train doors and windows is inconsistent, the thickness of the leak holes in the doors and windows is also inconsistent. As a comparison and verification, we also conducted research on the situations where the thickness of leak holes in doors and windows is consistent, and the thickness of leak holes in doors and windows is inconsistent. The different thicknesses of leak holes in doors and windows is shown in Fig. 15.

The pressure relief time after changing the door and window leak hole area ratio at two different thicknesses is shown in Fig. 16(a). It can be seen that when the thickness of the door and window leak holes are the same, the difference in the pressure relief time calculated by different door and window leak hole area ratios is only 0.3 s, at most. In this case, the impact of the door and window area ratio on the pressure relief time, is less than 3%. When the thickness of the door and window leak holes is different, reducing the area ratio of the door and window leak holes will increase the pressure relief time. When the door and window leak hole area ratio is reduced from 3:1 to 1:3, the pressure relief time increases by 1.23 s. Fig. 16(b) shows the pressure time history curves after changing the door and window leak hole area ratios for two different thicknesses. As can be seen, when the thickness of the door and window leak holes are the same, changing the area ratio of the door and window leak holes

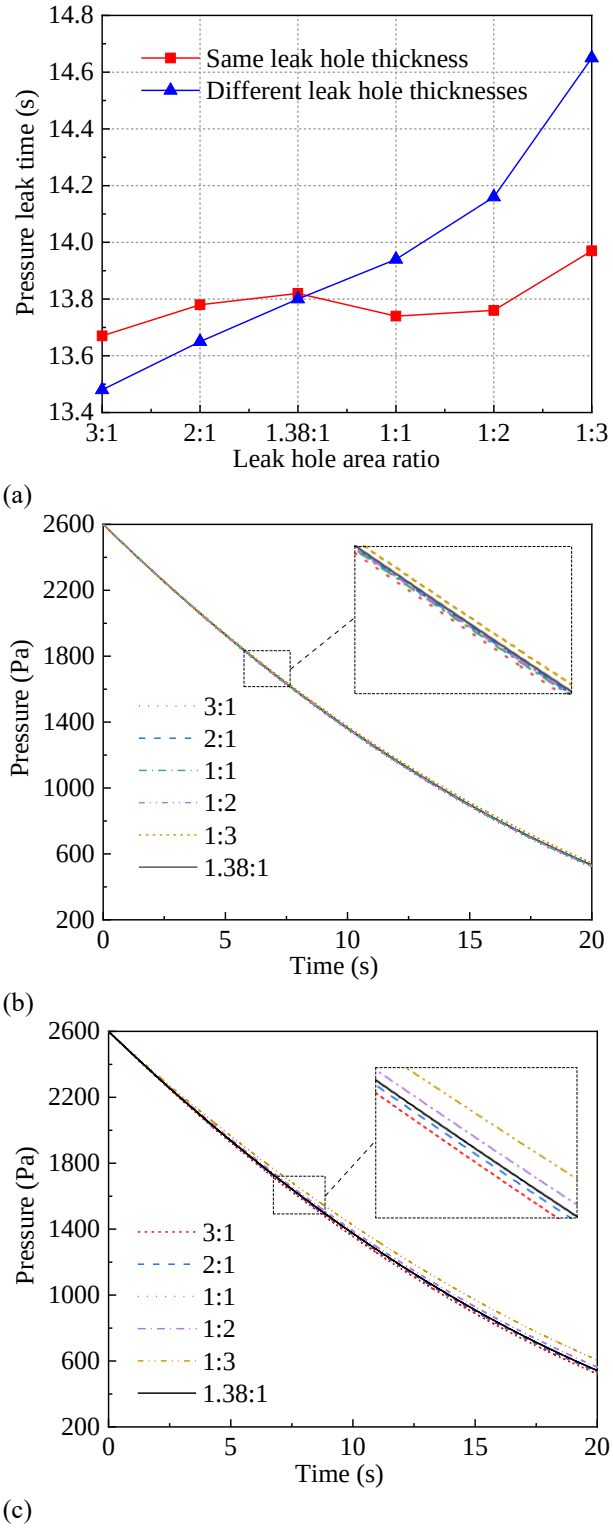

Fig. 16 Comparison of leakage characteristics when changing the area ratio of door and window leak holes: (a) Pressure relief time (b) Same door and window leak hole thickness (c) Different door and window leak hole thickness

will not have a big impact on the pressure leakage in the car, and the difference in the pressure curve will be small. However, when the thickness of the door and window leak holes is different, the smaller the area ratio of the door and window leak holes, the slower the pressure decreases, and the longer the pressure relief time.

Due to the different thicknesses of door and window structures, changing the area ratio of door and window leak holes will have a certain impact on the static leakage characteristics of the train. When the area ratio of door and window leak holes decreases, the area of the smaller-thickness window leak holes increases, and the area of the larger-thickness door leak holes decreases. According to the research results in 4.1.2, the airflow speed is smaller when passing through a leak hole with a smaller thickness. Therefore, compared with a leak hole with the same area, but a larger thickness, the mass flow rate is lower. In engineering, we can focus on and improve the sealing performance of thicker parts, such as train doors. When necessary ventilation holes or drainage holes need to be arranged on the carriage, we can choose to make holes in the thinner body parts, which will have less impact on the static airtightness of the train.

5. CONCLUSION

The influence of parameters of train leak holes on static airtightness was studied. The accuracy of the numerical simulation was validated through theoretical formulae and experimental data. The influence of the slenderness ratio and thickness of the leak hole on the airtightness of the train was analyzed in the case of a single leak hole, as was the influence of the number, location, slenderness ratio, and area ratio of the multiple leak holes, on the airtightness of the train. The conclusions reached are as follows:

(1) The velocity of airflow in the leak hole cross-section is distributed with a large center and small surroundings. Therefore, the slenderness ratio of the leak hole has a greater impact on the flow coefficient, which in turn affects the theoretical pressure relief time. The relative error between the pressure relief time obtained by numerical simulation, and the theoretical pressure relief time is the smallest. The errors for the case of a single leak hole and multiple leak holes are 4.93% and 3.68%, respectively. For numerical simulation, it is more appropriate to choose a leak hole with a slenderness ratio of 1:16.

(2) The airflow accelerates in the leak hole flow channel, as a result of the pressure differential. When the thickness of the leak holes does not exceed 200 mm, as the thickness of the leak holes increases, the velocity of airflow in the flow channel increases, and the pressure relief time decreases from 16.21 s to 12.98 s. As the thickness of the leak hole increases beyond 200mm, the maximum speed of the airflow no longer increases, the flow channel resistance increases, and the pressure relief time increases from 12.98 s to 13.47 s.

(3) When the total area of leak holes remains unchanged, the alteration of the number of leak holes has a minimal impact on the pressure relief time, and the maximum difference in pressure relief time is only 0.24 s. Changing the location of the leak holes does not affect the pressure relief time, but has a slight effect on the mass flow rate of the leak holes.

(4) When the thickness of leak holes in doors and windows is the same, the total area of leak holes remains

unchanged, and changing the area ratio of leak holes in doors and windows has an impact on the pressure relief time of less than 3%. When the door leak holes are thicker than the window leak holes, the reduction in the area ratio of the door and window leak holes causes the pressure relief time to increase by up to 1.23 s.

This study is based on a subway vehicle. Although the airtightness requirements of on-ground vehicles are different from those of subway vehicles, the design and optimization of leak holes are essentially the same. The results of the study can provide a reference for deciding the locations and shapes of the openings in the bodies of subway vehicles and on-ground vehicles. Due to the higher speed of on-ground vehicles, the pressure difference between the vehicle's interior and exterior may be greater. The results of this paper are not sufficient to reflect the leakage characteristics of on-ground vehicles, so follow-up research will be carried out on high-speed train airtightness.

ACKNOWLEDGMENTS

This work was supported by National Natural Science Foundation of China (12372049)，Fundamental Research Funds for the Central Universities (2682023ZTPY036) and Independent Project of State Key Laboratory of Rail Transit Vehicle System (2023TPL-T06).

CONFLICT OF INTEREST

The authors declare that they have no known competing financial interests or personal relationships that could have appeared to influence the work reported in this paper.

AUTHORS CONTRIBUTION

Nianxun Li: Methodology, Software, Writing – Original Draft. **Haoran Meng:** Investigation, Validation. **Tian Li:** Conceptualization, Writing – Reviewing and Editing. **Jiye Zhang:** Funding acquisition, Resources.

REFERENCES

Chang, C., Li, T., Qin, D., & Zhang, J. (2021). On the scale size of the aerodynamic characteristics of a high-speed train. *Journal of Applied Fluid Mechanics*, *15*(1), 209-219. https://doi.org/10.47176/jafm.15.01.33041

Chen, C. J., He, Z. Y., Feng, Y. P., & Yang, L. (2022). Semi-empirical model of internal pressure for a high-speed train under the excitation of tunnel pressure waves. *Proceedings of the Institution of Mechanical Engineers, Part F: Journal of Rail and Rapid Transit*, *236*(7), 803-815. https://doi.org/10.1177/09544097211042721

Chen, X., Liu, T., Xia, Y., Li, W., Guo, Z., Jiang, Z., & Li, M. (2021). The evolution of airtight performance for a high-speed train during its long-term service. *Measurement*, *177*, 109319. https://doi.org/10.1016/j.measurement.2021.109319

Gawthorpe, R., Figura, G., & Robertson, N. (1994). *Pressure chamber tests of Passenger comfort in tunnels.* 8th International Conference on Aerodynamics and Ventilation of Vehicle Tunnels. Liverpool, UK.

GlÖckle, H. (1994). *Determining comfort limits with regard to pressure changes and operational experiences with pressure-tight vehicles.* 8th International Conference on Aerodynamics and Ventilation of Vehicle Tunnels. Liverpool UK,

He, Z. Y., Chen, C. J., Yang, L., & Wang, D.W. (2023). Internal pressure control for high-speed trains based on condition matching and performance iteration. *Transactions of the Institute of Measurement and Control*, *45*(6), 1089-1098. https://doi.org/10.1177/01423312221126229

He, Z., Chen, C., Wang, D., Hu, J., & Yang, L. (2022). Modelling and iterative learning control of internal pressure for high-speed trains under excitation of varying-amplitude tunnel pressure waves. *Proceedings of the Institution of Mechanical Engineers, Part F: Journal of Rail and Rapid Transit*, *236*(8), 887-898. https://doi.org/10.1177/09544097211046067

Hu, X., Kong, F., Liang, Y., Yu, M., Duan, X., & Mei, Y. (2020). Numerical simulation for influence of line spacing on crossing pressure wave of high-speed trains in tunnel. *Journal of Vibration and Shock* *39*(21), 80-88. https://doi.org/10.13465/j.cnki.jvs.2020.21.011

Kobayashi, M., Suzuki, Y., Akutsu, K., & Ozawa, S. (1998). Alleviating aural discomfort of passengers on Shinkansen by controlling airflow rate in ventilation system. *JSME International Journal Series B Fluids and Thermal Engineering*, *41*(4), 936-944. https://doi.org/10.1299/jsmeb.41.936

Li, C., Liu, M., Chang, R., Wang, X., Liu, W., & Zhang, H. (2022). Air pressure and comfort study of the high-speed train passing through the subway station. *Sustainable Cities and Society*, *81*, 103881. https://doi.org/10.1016/j.scs.2022.103881

Li, T., Dai, Z. Y., Zhang, J. Y., & Zhang, W. H. (2020). Theoretical model and calculation of static leakage for train air tightness. *Journal of Traffic and Transportation Engineering*, *20*(1), 150-158. https://doi.org/10.19818/j.cnki.1671-1637.2020.01.012

Li, T., Qin, D., & Zhang, J. (2019a). Effect of RANS turbulence model on aerodynamic behavior of trains in crosswind. *Chinese Journal of Mechanical Engineering*, *32*, 1-12. https://doi.org/10.1186/s10033-019-0402-2

Li, T., Zhang, J. Y., Rashidi, M., & Yu, M. (2019b). On the reynolds-averaged navier-stokes modelling of the flow around a simplified train in crosswinds. *Journal of Applied Fluid Mechanics*, *12*(2), 551-563. https://doi.org/10.29252/jafm.12.02.28958

Li, W., Liu, T., Zhou, L., Chen, Z., Xia, Y., & Huo, X. (2023). Impact of ballast length on train aerodynamics for a wind tunnel layout via CFD analysis. *Alexandria Engineering Journal*, *65*, 275-293. https://doi.org/10.1016/j.aej.2022.10.040

Li, Y. J., & Mei, Y. G. (2009). Primary discussion about pressure tightness of electric multiple units. *Railway Locomotive & Car*, *29*(2), 31-35. https://doi.org/10.3969/j.issn.1008-7842.2009.02.008

Liang, H., Sun, Y., Li, T., & Zhang, J. (2022). Influence of marshalling length on aerodynamic characteristics of urban EMUs under crosswind. *Journal of Applied Fluid Mechanics*, *16*(1), 9-20. https://doi.org/10.47176/JAFM.16.01.1338

Liu, T. H., Chen, X. D., Li, W. H., Xie, T. Z., & Chen, Z.W. (2017). Field study on the interior pressure variations in high-speed trains passing through tunnels of different lengths. *Journal of Wind Engineering and Industrial Aerodynamics*, *169*, 54-66. https://doi.org/10.1016/j.jweia.2017.07.004

Liu, T., Chen, M., Chen, X., Geng, S., Jiang, Z., & Krajnović, S. (2019). Field test measurement of the dynamic tightness performance of high-speed trains and study on its influencing factors. *Measurement*, *138*, 602-613. https://doi.org/10.1016/j.measurement.2019.02.051

Liu, T., Geng, S., Chen, X., & Krajnovic, S. (2020). Numerical analysis on the dynamic airtightness of a railway vehicle passing through tunnels. *Tunnelling and Underground Space Technology*, *97*, 103286. https://doi.org/10.1016/j.tust.2020.103286

Lu, Y., Wang, T., Yang, M., & Qian, B. (2020). The influence of reduced cross-section on pressure transients from high-speed trains intersecting in a tunnel. *Journal of Wind Engineering and Industrial Aerodynamics*, *201*, 104161. https://doi.org/10.1016/j.jweia.2020.104161

Nam, S. W. (2004). A study on the characteristics of internal and external pressure variation for KTX. *Journal of the Korean Society for Railway*, *7*(1), 26-31. https://doi.org/10.13078/jksrs.04014

Nam, S. W. (2016). a study on estimation of air tightness for train. *Journal of the Korean Society for Railway*, *19*(5), 576-584. https://doi.org/10.7782/JKSR.2016.19.5.576

Niu, J., Lv, D., Li, R., Zhou, D., Wang, Y., & Yang, X. (2023). Matching of multiple aerodynamic parameters for railway train/tunnel systems to ensure critical airtightness performance of high-speed trains. *Structural and Multidisciplinary Optimization*, *66*(1), 4. https://doi.org/10.1007/s00158-022-03462-z

Raghunathan, R. S., Kim, H. D., & Setoguchi, T. (2002). Aerodynamics of high-speed railway train. *Progress in Aerospace Sciences*, *38*(6-7), 469-514. https://doi.org/10.1016/S0376-0421(02)00029-5

Saiprakash, M., SenthilKumar, C., Sunil, G., Rampratap, S., Shanmugam, V., & Balu, G. (2019). Visualization of shock wave phenomenon around a sharp cone model at hypersonic mach number in a shock tunnel using high speed schlieren facility. *Journal of Applied Fluid Mechanics*, *12*(2), 461-468. https://doi.org/10.29252/jafm.12.02.29250

Su, X., Cheng, J., & Han, Z. (2004). Survey on research of air-tightness of high-speed trains. *Rail Locomot*, *42*, 16-19. https://doi.org/10.3969/j.issn.1002-7602.2004.05.005

Wei, L., Zeng, J., Huang, C., Zheng, B., & Li, X. (2024). Hunting stability and dynamic stress analysis of a high-speed bogie using elastic-suspended motors as dynamic vibration absorber. *Vehicle System Dynamics*, 1-23. https://doi.org/10.1080/00423114.2023.2289654

Wu, Z., Zhou, D., Li, S., Yang, J., Chen, G., & Li, X. (2022). Numerical analysis of the effect of streamlined nose length on slipstream of high-speed train passing through a tunnel. *Journal of Applied Fluid Mechanics*, *15*(6), 1933-1945. https://doi.org/10.47176/JAFM.15.06.1189

Xu, L., Liang, X., Liu, T., & Xiong, X. (2014). Pressure variation test inside full-scale high-speed train running in open area. *Zhongnan Daxue Xuebao (Ziran Kexue Ban)/Journal of Central South University (Science and Technology)*, *45*(8), 2878-2884. http://zkxb.csu.edu.cn/thesisDetails?columnId=3395086&Fpath=home&index=0&lang=zh

Zhou, M. M., Liu, T. H., Xia, Y. H., Li, W. H., & Chen, Z. H. (2022). Comparative investigations of pressure waves induced by trains passing through a tunnel with different speed modes. *Journal of Central South University*, *29*(8), 2639-2653. https://doi.org/10.1007/s11771-022-5098-2